RSC Advances

PAPER

View Article Online
View Journal | View Issue

Cite this: *RSC Adv.*, 2019, **9**, 37109

The effective photocatalysis and antibacterial properties of AgBr/$AgVO_3$ composites under visible-light

Jie Zhang,[*abd] Jia Wang,[abcd] Huihui Xu,[*abcd] Xianzi Lv,[abd] YuXiang Zeng,[a] Jizhou Duan[abd] and Baorong Hou[abd]

Received 28th August 2019
Accepted 5th November 2019

DOI: 10.1039/c9ra06810d

rsc.li/rsc-advances

With the discharge of large amount of organic pollutants and antibiotics into the water environment, the water cycle has been seriously polluted, and at the same time, various drug-resistant bacteria have emerged in succession, which poses a serious threat to human health. In recent years, photocatalytic nanomaterials have become a research hotspot in the antimicrobial area. In this study, AgBr/$AgVO_3$ photocatalysts were prepared by a hydrothermal process and an *in situ* growth method. The composites were tightly connected by the (501) plane of $AgVO_3$ and the (200) lattice plane of AgBr. The photocatalytic activity was tested by degrading Rhodamine B (RhB) solution under visible-light, and the result indicated that the photodegradation rate for RhB solution was 92.3% by the photocatalysis with 0.5AgBr/$AgVO_3$ and the photocatalytic performance of 0.5AgBr/$AgVO_3$ was improved compared to pure $AgVO_3$ and AgBr. In addition, more than 99.997% of *E. coli*, *S. aureus*, and *P. aeruginosa* cells were killed by the photocatalysis with 0.5AgBr/$AgVO_3$ within 30 min. These results demonstrated that the 0.5AgBr/$AgVO_3$ heterojunction photocatalyst could be widely used in the treatment of environmental pollution and in the antibacterial field.

Introduction

In order to realize the effective utilization of solar energy and reduce the harm of antimicrobial materials to the environment and human beings, it is of great significance to develop and design green environment-friendly photocatalytic antimicrobial materials. In recent years, photocatalytic nanomaterials have become a research hotspot in the field of antimicrobials[1–8] because of their good broad-spectrum antimicrobial properties, lack of secondary pollution and stability. Many studies have examined the antibacterial properties of photocatalysts on *E. coli*,[1,3–5,8] *S. aureus*,[1,8] *P. aeruginosa*,[6] *Lactobacillus*[2] and Sulfate Reducing Bacteria.[2]

Under light irradiation, the semiconductor will generate electrons and holes which react with water or air to form reactive oxygen species ($\cdot OH^-$, $\cdot O_2^-$, h^+).[1,7] These free radicals will destroy the cell walls and cell membranes of microbial cells, lead to the leakage of cytoplasm and cause the apoptosis of microbial cells. At the same time, these free radicals can also enter the cell, destroy the functional macromolecules in the cell, cause the disorder of growth and metabolism of microbial cells, and further oxidize and decompose microbial metabolites and intracellular substances, so as to achieve the complete killing of microorganisms.

Currently, $AgVO_3$ (p-type semiconductor) material has received increasing attention because of its narrow band gap, stable structure, excellent photocatalytic performance and potential applications in batteries and sensors.[8,9] However, because of its high recombination rate of photoelectron–hole pairs, it's necessary to enhance the photocatalytic performance by forming heterojunctions between $AgVO_3$ and other semiconductors. Some scholars have designed $AgVO_3$-based composites, such as Ag/$AgVO_3$/RGO,[10] $InVO_4$/$AgVO_3$,[8] and $AgVO_3$/MoS_2.[11] And the above composites are mainly used for degrading poisonous chemicals, and rarely used to sterilize. At the same time, AgBr (n-type semiconductor)[12] has been widely investigated as co-catalyst because of its excellent photocatalytic activity. Therefore, our goal is to obtain AgBr/$AgVO_3$ composite with excellent activity and stability that can be used in photocatalytic antibacterial area and water purification applications.

In this work, AgBr/$AgVO_3$ photocatalysts with different molar ratios were prepared *via* a hydrothermal process and an *in situ* growth method. The morphology, structure and composition of AgBr/$AgVO_3$ nanocomposites were revealed by X-ray powder diffraction (XRD), scanning electron microscopy (SEM),

[a]*Key Laboratory of Marine Environmental Corrosion and Bio-fouling, Institute of Oceanology, Chinese Academy of Sciences, 7 Nanhai Road, Qingdao, 266071, China. E-mail: zhangjie@qdio.ac.cn; xuhuihui16@mails.ucas.ac.cn; Fax: +86-532-82880498; Tel: +86-532-82898851*

[b]*Open Studio for Marine Corrosion and Protection, Pilot National Laboratory for Marine Science and Technology, Qingdao 266237, China*

[c]*University of Chinese Academy of Sciences, Beijing, 100049, China*

[d]*Center for Ocean Mega-Science, Chinese Academy of Sciences, Qingdao, 266071, China*

transmission electron microscopy (TEM), nitrogen (N_2) absorption (BET specific surface area) and X-ray photoelectron spectroscopy (XPS). The photocatalytic activities of AgBr/$AgVO_3$ composites were tested by degrading organic pollutants RhB solution. And the antibacterial activity was determined by killing *E. coli*, *S. aureus*, and *P. aeruginosa*, which were used as model bacteria. Moreover, a mechanism for the photocatalytic reactions of AgBr/$AgVO_3$ heterojunction was proposed based on the above experimental data.

Experimental section

Chemicals

$AgNO_3$, NH_4VO_3, NaBr, HNO_3, $NH_3 \cdot H_2O$, Rhodamine B (RhB), isopropyl alcohol (IPA), benzoquinone (BQ) and sodium oxalate (MSDS) were used. All the reagents were of analytical grade and used as received without further purification. *P. aeruginosa* (a Gram-negative bacteria), *E. coli* (a Gram-negative bacteria) and *S. aureus* (a Gram-positive bacteria) were obtained from the Institute of Oceanology, Chinese Academy of Sciences (Qingdao, China).

Synthesis of AgBr/$AgVO_3$ photocatalysts

$AgVO_3$ samples were synthesized *via* a hydrothermal process as follows: 0.34 g $AgNO_3$ was dissolved in 30 ml distilled water under magnetic stirring to obtain solution A, and 0.234 g NH_4VO_3 was dissolved in 30 ml distilled water to obtain solution B. Solution A was added dropwise to solution B and the pH of the final suspension was adjusted to 7.0 with 2.0 M HNO_3 and $NH_3 \cdot H_2O$. The mixture was transferred into a 100 ml Teflon-lined stainless steel autoclave, which was heated to 180 °C for 24 h.[13] The products were cooled to room temperature and washed with water and ethanol and collected after filtering. Finally, the samples were dried at 60 °C a vacuum oven for 12 h to obtain pure $AgVO_3$ crystals with one-dimensional rod-like nanostructures. The rod-like structure of $AgVO_3$ was selected because the one-dimensional nanostructure exhibited photocatalytic activity superior to that of nanosheet structure.[14]

For the synthesis of AgBr/$AgVO_3$ photocatalysts: 0.2068 g $AgVO_3$ powder was dispersed into 30 ml absolute ethanol and sonicated for 60 min. After that, 0.085 g $AgNO_3$ was dissolved into the solution and stirred magnetically for another 30 min. NaBr (0.0514 g) was dissolved in 20 ml deionized water and added dropwise into the above solution under constant magnetic stirring and then stirred for another 3 h in the dark. The precipitate was filtered and washed with deionized water and ethanol. The final product was dried at 60 °C for 12 h in the dark. The sample was denoted as "0.5AgBr/$AgVO_3$". Using this method, AgBr/$AgVO_3$ photocatalysts with different molar ratios were prepared and termed as 0.1AgBr/$AgVO_3$, 0.3AgBr/$AgVO_3$, 0.5AgBr/$AgVO_3$ and 0.7AgBr/$AgVO_3$. For comparison, AgBr photocatalyst was also prepared using the similar method.

Characterization

The phase purity and components of the AgBr/$AgVO_3$ photocatalysts were characterized by XRD (Rigaku D/max-3C, Japan) operating at 40 kV and 30 mA with Cu Kα radiation ($\lambda = 0.15406$ nm). TEM and HRTEM images were taken on a Tecnai G220 transmission electron microscope at 200 kV acceleration voltage. The nitrogen (N_2) adsorption–desorption measurements were conducted at 77 K by use of Micromeritics ASAP2020, and the sample was degassed at 200 °C for 6 h to remove physisorbed gases. The Brunauer–Emmett–Teller (BET) approach using adsorption data was followed to evaluate the specific surface area. The X-ray photoelectron spectroscopy (XPS) measurements were measured using a Multifunctional imaging electron spectrometer (Thermo ESCALAB 250XI, USA). The UV-vis diffuse reflectance spectra (UV-DRS) of the samples were tested using a Hitachi U-3900H Spectrometer (Japan) using $BaSO_4$ as the reference.

Photocatalytic performance

In this paper, RhB was selected as a model pollutant to determine the catalytic performance of the heterostructures, and an 800 W xenon lamp[15] was used as the visible light source (XPA-7, Xujiang Electromechanical Plant, Nanjing, China). And the wavelength range of the final output light was 420–780 nm, which coincided with the range of visible light. In this experiment, 30 mg of the catalysts were added to 50 ml of RhB (10 mg l^{-1}) solution. The solution was stirred for 30 min in the dark to ensure the establishment of an adsorption–desorption equilibrium.[1] During the irradiation, 4 ml of the suspension was collected and analyzed after centrifugation at regular intervals. The concentration of RhB solution was determined using a TU-1901 spectrometer. The RhB photodegradation process was approximated by the following pseudo-first-order kinetic model:[16] $\ln(C_t/C_0) = kt$, where t is the reaction time, C_t is the organic pollutant concentrations at reaction time t, C_0 is the initial concentration, and the rate constant k is the slope of the corresponding fitted curves.

Photocatalytic antibacterial experiments

In the antibacterial experiment, an 800 W Xe lamp was used as the light source, and *E. coli*, *S. aureus* and *P. aeruginosa* were used as model bacteria.[15] Typically, 20 mg of photocatalyst,

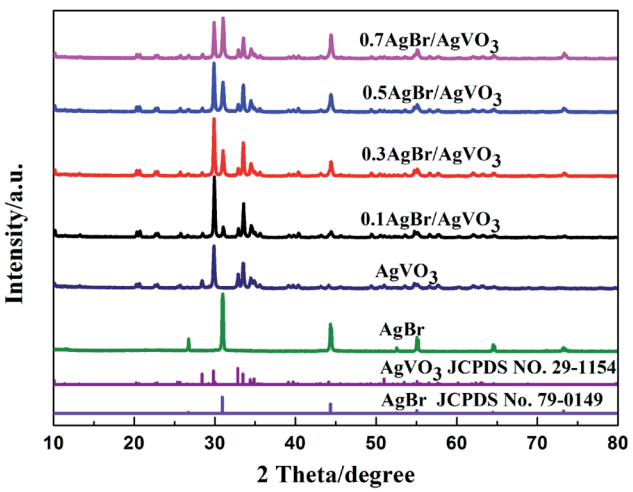

Fig. 1 XRD patterns of AgBr/$AgVO_3$ heterostructures with different molar ratios.

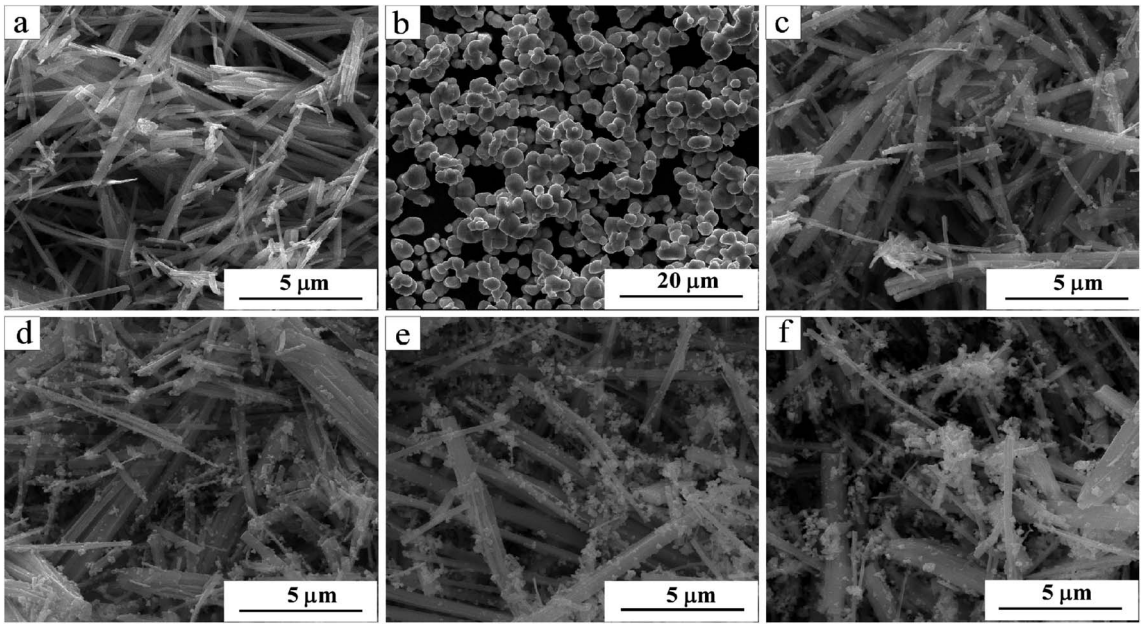

Fig. 2 SEM images of as-synthesized samples: (a) pure $AgVO_3$, (b) pure AgBr, (c) 0.1AgBr/$AgVO_3$, (d) 0.3AgBr/$AgVO_3$, (e) 0.5AgBr/$AgVO_3$, (f) 0.7AgBr/$AgVO_3$.

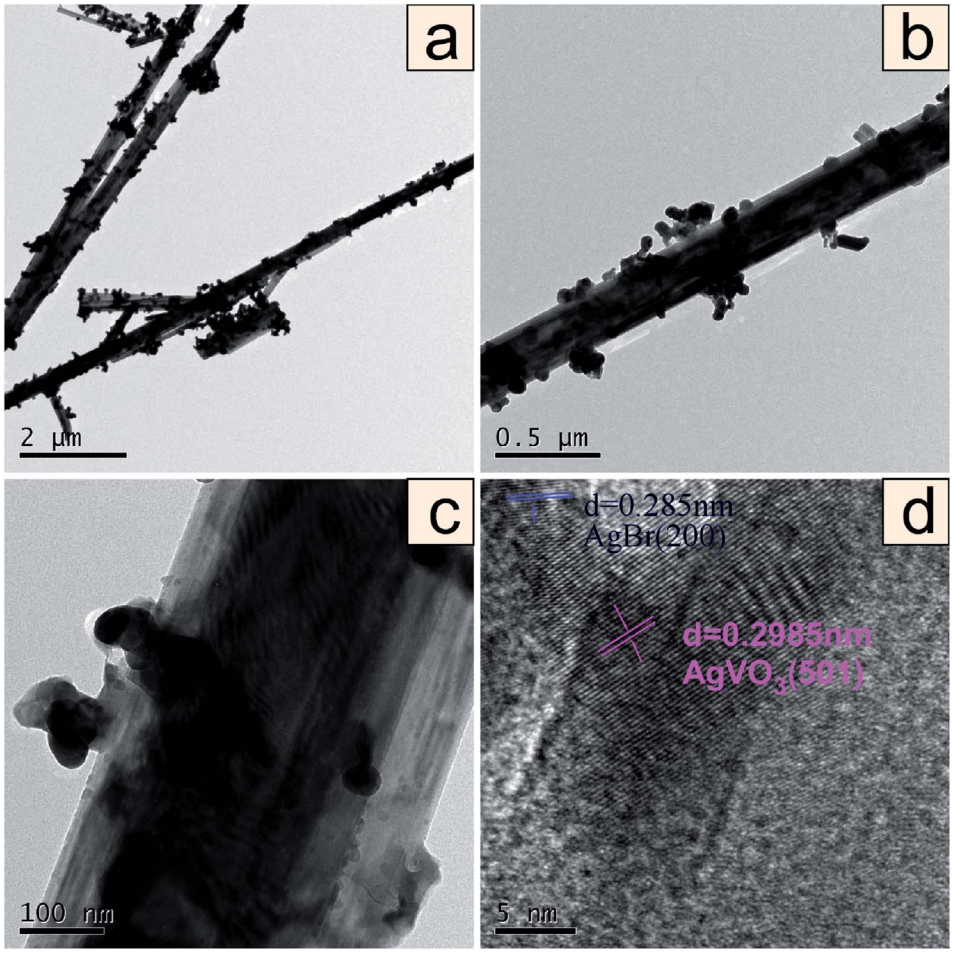

Fig. 3 TEM images in low magnification (a and b), high magnification (c) and the corresponding HRTEM image of 0.5$AgVO_3$/AgBr (d).

Table 1 The specific surface area of different samples

Sample	$S_{BET}/(m^2\ g^{-1})$
AgBr	3.8990
$AgVO_3$	9.0904
$0.1AgBr/AgVO_3$	23.3675
$0.3AgBr/AgVO_3$	35.0681
$0.5AgBr/AgVO_3$	21.7348
$0.7AgBr/AgVO_3$	11.1933

45 ml of sterilized natural seawater, and 5 ml of bacterial suspension were added to 50 ml quartz tubes in sequence. The suspension was magnetically stirred for 30 min in the dark to establish an adsorption–desorption equilibrium. During the irradiation, 1 ml of the suspension was collected and diluted with sterilized seawater. Then, 100 μl of the diluted suspension was dropped on LB or 2216E agar plates. After incubation at 37 °C for 24 h, the number of bacterial colonies (in cfu) were calculated. The antibacterial rate was computed as follows:[1,7]

$$\text{survival rate } (\%) = (N_t/N_0) \times 100\%.$$

Where: N_0 is the numbers of viable cells in original bacterial solution, N_t is the numbers of viable cells in bacterial solution after reaction. The antibacterial rate was defined as follows:

$$\text{antibacterial rate } (\%) = 100 - \text{survival rate}.$$

Results and discussion

The structural analysis of photocatalysts

The crystal phase and structure of the photocatalysts were determined by XRD, and the XRD patterns were shown in Fig. 1. The pure $AgVO_3$ sample showed diffraction peaks at $2\theta = 28.4°$, 29.8°, 32.8°, 33.5°, 34.4°, 34.9° and 50.9°, which can be indexed to the $AgVO_3$ (−211), (501), (−411), (−112), (−602), (112) and (020) planes (JCPDS No. 29-1154).[8] For pure AgBr, strong peaks occurred at $2\theta = 30.9°$, 44.3°, 55.0° and 73.2°, which can be indexed to the AgBr (200), (220), (222) and (420) planes (JCPDS No. 79-0149).[17] The $AgBr/AgVO_3$ photocatalysts had characteristic diffraction peaks that could be indexed to monoclinic-phase $AgVO_3$ (JCPDS No. 29-1154) and cubic-phase AgBr (JCPDS No. 79-0149). In addition, the intensities of the diffraction peaks of AgBr increased gradually with the increase of the AgBr concentration in the $AgBr/AgVO_3$ composites, while those of $AgVO_3$ decreased as its content decreased. No peaks of other samples were shown in the $AgBr/AgVO_3$ composites, indicating that the composites were only composed of AgBr and $AgVO_3$.

Characterization of the photocatalysts

Fig. 2(a–f) showed the SEM images of pure $AgVO_3$, AgBr and $AgBr/AgVO_3$ samples with different molar ratios. As shown in Fig. 2(a), pure $AgVO_3$ exhibited a rod-like structure, with a diameter of approximately 500 nm, and the shape of pure AgBr crystals were irregular (Fig. 2(b)). The $AgBr/AgVO_3$ heterostructure was a rod-like structure with spherical shapes, as shown in Fig. 2(c–f). With the increase of molar ratio of AgBr, the amount of AgBr particles attached to the rod-like $AgVO_3$ increased. When the loading was large, the AgBr particles aggregated into a cluster and accumulated on the rod structure.

In order to further investigate the microstructure of the $0.5AgBr/AgVO_3$ composite, TEM, HRTEM were carried out. It can be seen that the $0.5AgBr/AgVO_3$ composite had a rod-like structure with irregular particles in Fig. 3(a and b). In addition, the enlarged TEM image in Fig. 3(c) clearly showed the rod-like structure (diameters of approximately 500 nm) with irregular particles (an average size of 50 nm). The HRTEM image (Fig. 3(d)) showed clearly two sets of different lattice fringes with calculated spaces of 0.2985 nm and 0.2850 nm, which were in

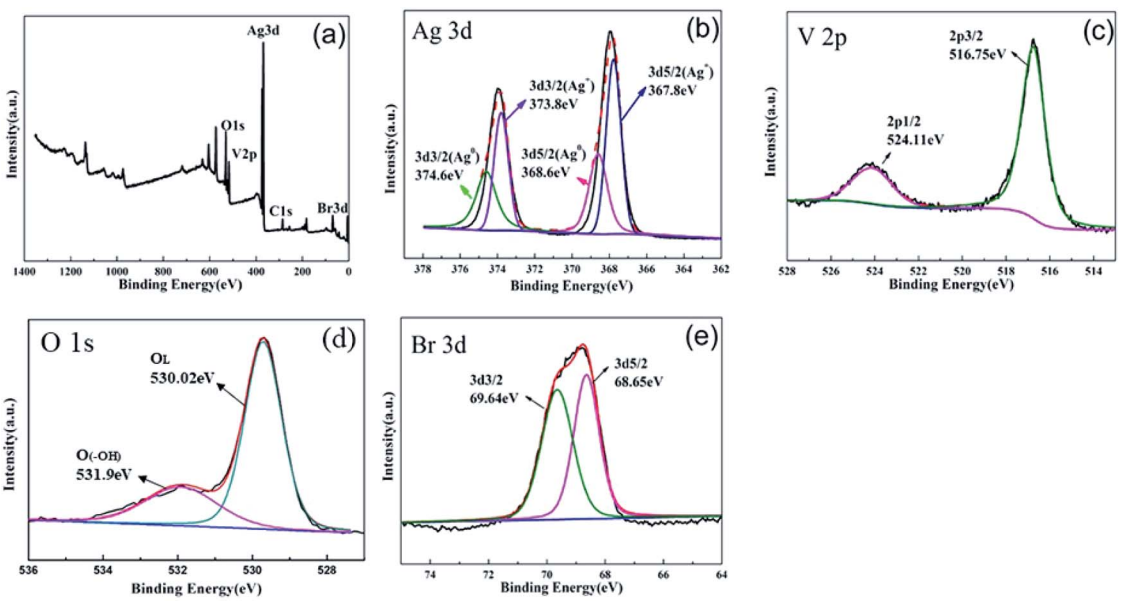

Fig. 4 XPS spectra of $0.5AgBr/AgVO_3$ composition: (a) survey, (b) Ag 3d, (c) V 2p, (d) O 1s, and (e) Br 3d.

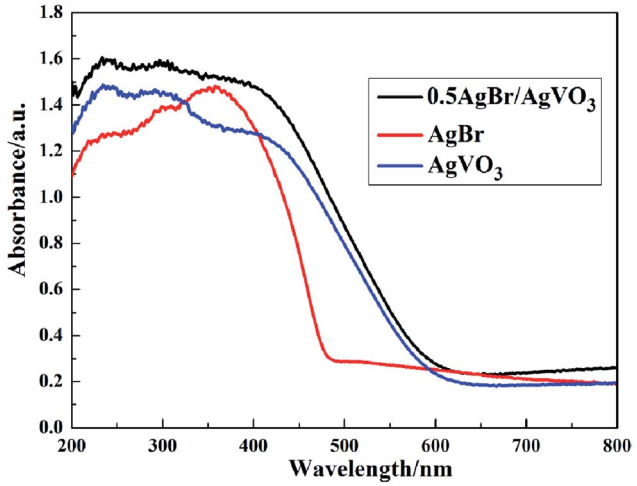

Fig. 5 UV-vis diffuse reflectance spectra of composites.

agreement with the (501) lattice plane of the tetragonal $AgVO_3$ (ref. 8 and 10) and (200) lattice plane of the orthorhombic AgBr,[18,19] respectively. The result demonstrated that a well-defined heterojunction structure was formed between AgBr and $AgVO_3$, which was consistent with the XRD results.

The BET specific surface area data of different proportion of photocatalysts was shown in Table 1. The specific surface area of the 0.3 $AgBr/AgVO_3$ composite photocatalyst was the largest, with a value of 35.0681 $m^2\ g^{-1}$. When the doping ratio of AgBr was further increased, the specific surface area of the photocatalyst decreases and the specific surface areas of 0.5AgBr/$AgVO_3$ and 0.7AgBr/$AgVO_3$ were 21.7348 $m^2\ g^{-1}$ and 11.1933 $m^2\ g^{-1}$ respectively. The reason was that coalescence of AgBr nanoparticles resulted in the grain growth and the specific surface area reduction for 0.5AgBr/$AgVO_3$ and 0.7AgBr/$AgVO_3$.[20] Fig. 2 can provide us with the basis for speculation. It can also be seen from Fig. 2 that pure AgBr nanoparticles cluster together, thus the specific surface area of AgBr is small. Above all, coupling AgBr with $AgVO_3$ promotes the specific surface area of $AgVO_3$. High specific surface area is more conducive to the diffusion and adsorption of pollutants and increase the reaction sites, thus further improving its catalytic activity.[21,22]

XPS spectra of 0.5AgBr/$AgVO_3$ composite were obtained to investigate the elemental composition and valence states. As shown in Fig. 4(a), XPS survey spectrum (Fig. 4(a)) revealed the presence of Ag 3d, V 2p, Br 3d and O 1s electronic states in the composite. Fig. 4(b) showed a high-resolution XPS spectrum of Ag 3d, and there were two peaks at 367.8 eV and 373.8 eV corresponding to Ag $3d_{5/2}$ and Ag $3d_{3/2}$, respectively, which can be attributed to Ag^+ of AgBr or $AgVO_3$.[8] And the peaks at 368.6 and

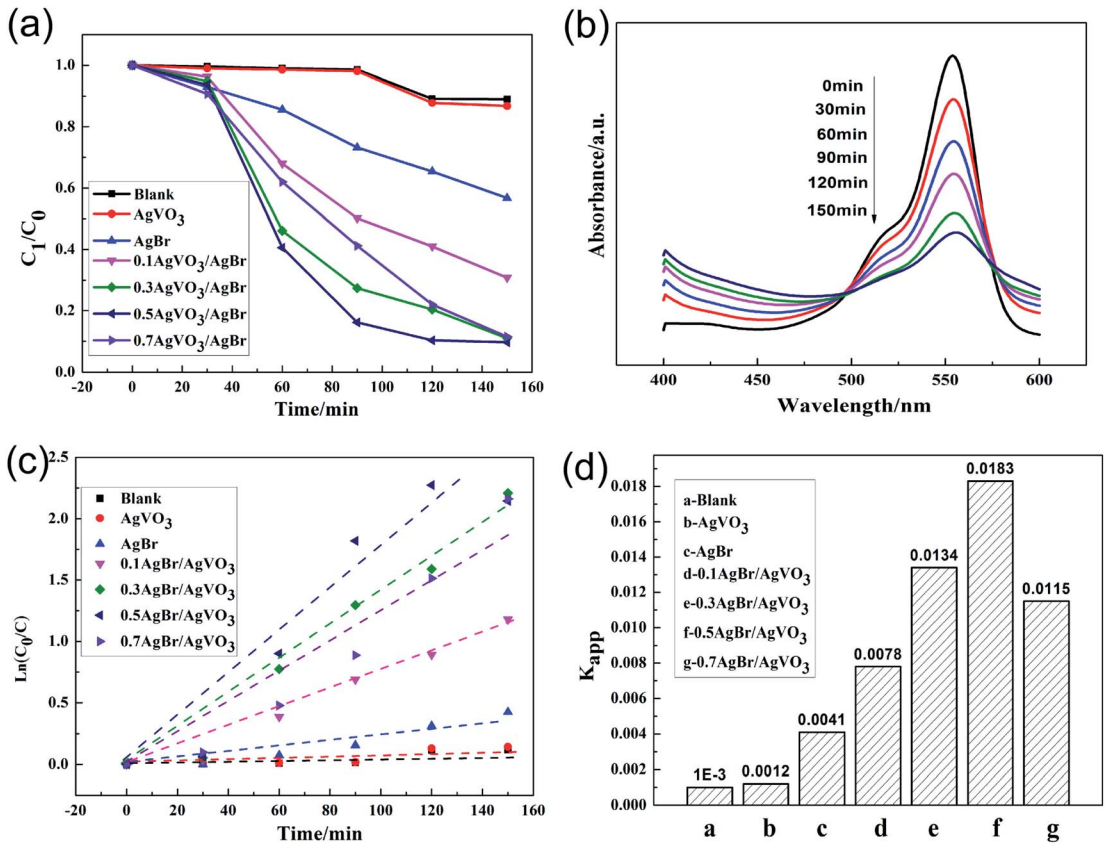

Fig. 6 (a) Photocatalytic degradation curves of RhB solution for different photocatalysts; (b) UV-DRS of RhB solutions at different time with 0.5AgBr/$AgVO_3$; (c) the first-order kinetics of RhB degradation in the presence of different photocatalysts; (d) the degradation rate constant of RhB with different samples.

374.6 eV can be ascribed to Ag^0 species, according to previous report[19] which further verified the existence of Ag^0 in AgBr/$AgVO_3$. The spectrum of V 2p (Fig. 4(c)) showed that the signals for V $2p_{1/2}$ and V $2p_{3/2}$ were approximately 524.11 eV and 516.75 eV, respectively, corresponding to V^{5+} in $AgVO_3$.[7,19] The spectrum of Br 3d was shown in Fig. 4(e), and there were two peaks at 68.65 eV and 69.64 eV, which were consistent with Br $3d_{5/2}$ and Br $3d_{3/2}$ peaks,[18,19] corresponding to Br^- in AgBr. The Br/V molar ratio was calculated as 0.619 by sensitivity factor method, which is 23.8% higher than its nominal composition (0.5), and it indicates that bromine atoms are really dispersed on the catalysts surface. The oxygen peak is generally fitted by two components, respectively corresponded to oxygen in the oxide lattice and surface OH groups or undissociated water.[14] Fig. 4(d) presents the high resolution XPS spectrum O 1s peaks. The peaks situated at 530.02 eV and 531.9 eV can be attributed to V–O and the –OH on the surface of the samples. Yang Xu *et al.* obtained similar results to ours for XPS spectrum of O 1s.[23] According to Fig. 4(d), the ratio of the surface –OH to the total oxygen components can be estimated roughly to be 28.9%. The resultant abundant surface hydroxyl groups have been confirmed the strong chemical interaction between AgBr/$AgVO_3$. The presence of hydroxyl groups also contributes to the photocatalytic reactions, because they can act as capture centers for photoinduced electrons. Overall, the XPS results confirmed that AgBr and $AgVO_3$ coexisted in the AgBr/$AgVO_3$ composites.

The UV-vis diffuse reflectance spectra was measured to study the photophysical properties of AgBr/$AgVO_3$ samples. It can be seen that the initiation of the adsorption edge of $AgVO_3$ was approximately 610 nm in Fig. 5. And it was calculated that the optical band-gap energy of $AgVO_3$ was 2.03 eV (ref. 8) by using the equation $E_g = 1240/\lambda$. Simultaneously, the initiation of the adsorption edge of AgBr was approximately 480 nm, corresponding to a 2.58 eV band gap.[18,19,24] After loading AgBr, the absorption band edge showed a significant shift to the visible-light region because of the synergistic effect between AgBr and $AgVO_3$.

The photocatalytic activity

The activity of the catalysts was evaluated by comparing the degradation rates of RhB solution under visible light irradiation. The photocatalytic performances of AgBr/$AgVO_3$ catalysts were shown in Fig. 6. As shown in Fig. 6(a), in the blank experiment, the degradation rate of RhB solution was very low, therefore the effects of visible light and other environmental factors did not need to be considered in the results.[1,25] In addition, it can be seen that the 0.5AgBr/$AgVO_3$ photocatalyst had a higher degradation efficiency compared to pure $AgVO_3$ and AgBr/$AgVO_3$ compositions with other molar ratios under visible light in Fig. 6(a). In Fig. 6(b), the maximum absorbance of RhB solution was at 554 nm,[26] and the peak intensity at 554 nm decreased progressively by the photocatalysis of 0.5AgBr/$AgVO_3$ composites under visible light. After 150 min of irradiation, 92.3% of the RhB was degraded. In Fig. 6(c and d), the pseudo-first-order reaction kinetic constant K_{app}[27] of RhB was 0.0183 min^{-1} by the photocatalysis of 0.5AgBr/$AgVO_3$, which was 15 times higher than that of pure $AgVO_3$.

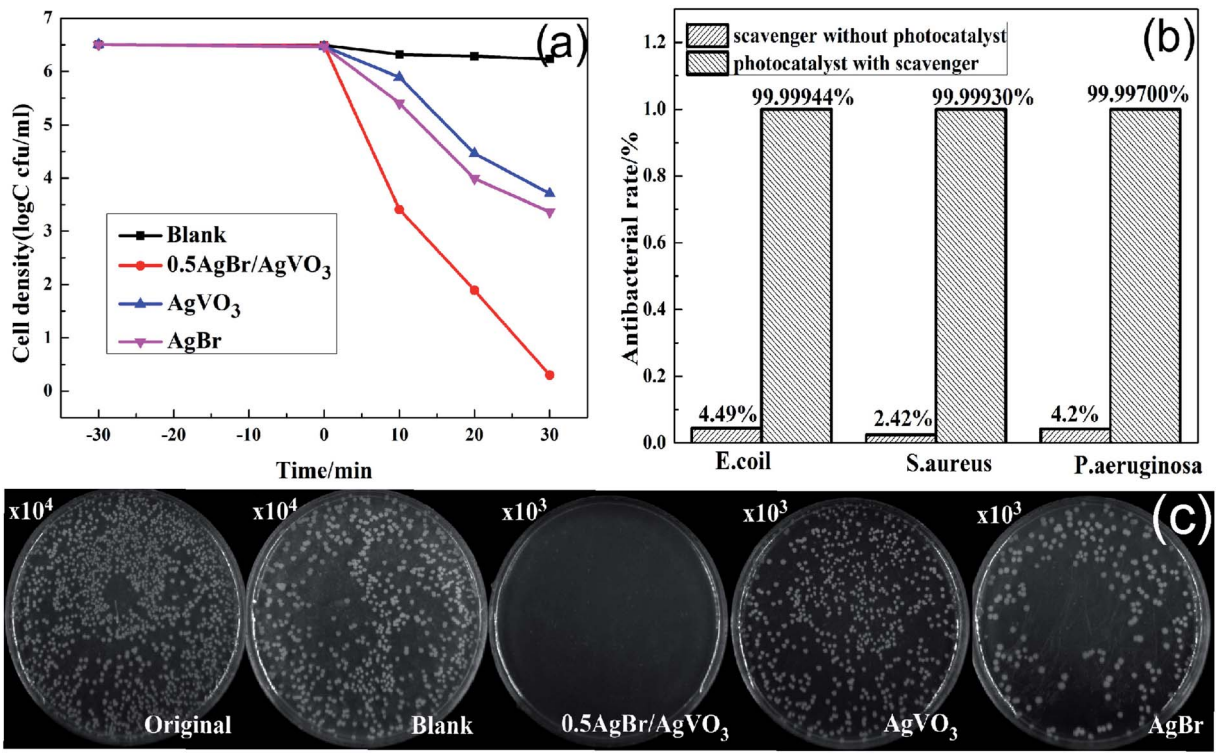

Fig. 7 (a) *P. aeruginosa* survival curves in the antibacterial experiments, (b) photocatalytic antibacterial rates of *E. coli*, *S. aureus* and *P. aeruginosa* with 0.5AgBr/$AgVO_3$ for 30 min, and the survival pictures of *P. aeruginosa* colonies in the presence of different photocatalysts (c).

Photocatalytic antibacterial efficiency

In this study, *P. aeruginosa* (3.2×10^6 cfu per ml), *E. coli* (3.54×10^7 cfu per ml) and *S. aureus* (1.4×10^7 cfu per ml) were chosen as model bacteria to evaluate the photocatalytic antibacterial activities of the prepared photocatalysts under visible light irradiation. As shown in Fig. 7(a), the survival curves of *P. aeruginosa* suggested that the number of bacterial cells remained constant in the blank experiments, indicating that there was no effect to the bacterial cells for photocatalysts in the dark. In addition, it can be seen in Fig. 7(a) that the 0.5AgBr/$AgVO_3$ photocatalysts exhibited enhanced photocatalytic antibacterial activities by comparison with pure AgBr and pure $AgVO_3$ under visible-light. In addition, the survival pictures of *P. aeruginosa* colonies in the presence of different photocatalysts were shown in Fig. 7(c). The photocatalytic performance of the 0.5AgBr/$AgVO_3$ compositions was improved because of the formation of the p–n heterojunction between AgBr and $AgVO_3$, which increased the separation of the photo-generated carriers. Moreover, it can be seen in Fig. 7(b) that most of the bacteria were killed, with anti-microbial rates of 99.99944%, 99.99930% and 99.99700% for *E. coli*, *S. aureus* and *P. aeruginosa* after 30 min by the photocatalysis of 0.5AgBr/$AgVO_3$.

Furthermore, compared to other reported antibacterial photocatalysts, such as BiOI/$BiVO_4$,[1] Cu_2O[28] and ZnO–Bi_2O_3,[29] the 0.5 AgBr/$AgVO_3$ composites showed better photocatalytic antibacterial activity, making it a potential photocatalyst in antibacterial area.

Stability and reusability

The stability and reusability of photocatalysts were important in practical application. Therefore, the antibacterial experiments of *P. aeruginosa* were repeated under visible light irradiation. After each circulation, the photocatalyst was collected by centrifugation, washed and dried for the next cycle. As shown in Fig. 8(a), after 6 cycles, the antibacterial rate of the 0.5AgBr/$AgVO_3$ composites did not decrease significantly which suggested good stability of the photocatalyst. Fig. 8(b) showed the XRD pattern of 0.5AgBr/$AgVO_3$ photocatalyst after 6 cycles. It can be seen that there was almost no change at all for the crystal phase and chemical composition of the photocatalyst after 6 cycles. Fig. 8(c) revealed the SEM image of the 0.5AgBr/$AgVO_3$ photocatalyst after 6 runs, and there is no apparent change in morphology, indicating the good stability of 0.5AgBr/$AgVO_3$.

Photocatalytic mechanism

To further confirm the role of the free radical active species for the photocatalytic reaction, the free radical trapping experiments were measured. 2-Propanol (IPA) was used as an $\cdot OH^-$ scavenger, sodium oxalate (MSDS) as a h^+ scavenger and 1,4-benzoquinone (BQ) as an $\cdot O_2^-$ scavenger.[1,7,8] As shown in Fig. 9, the degradation rate of RhB reached 92.3% after 150 min by the photocatalysis of 0.5AgBr/$AgVO_3$ without any scavenger. With the addition of 1 mmol IPA, the degradation rate of RhB

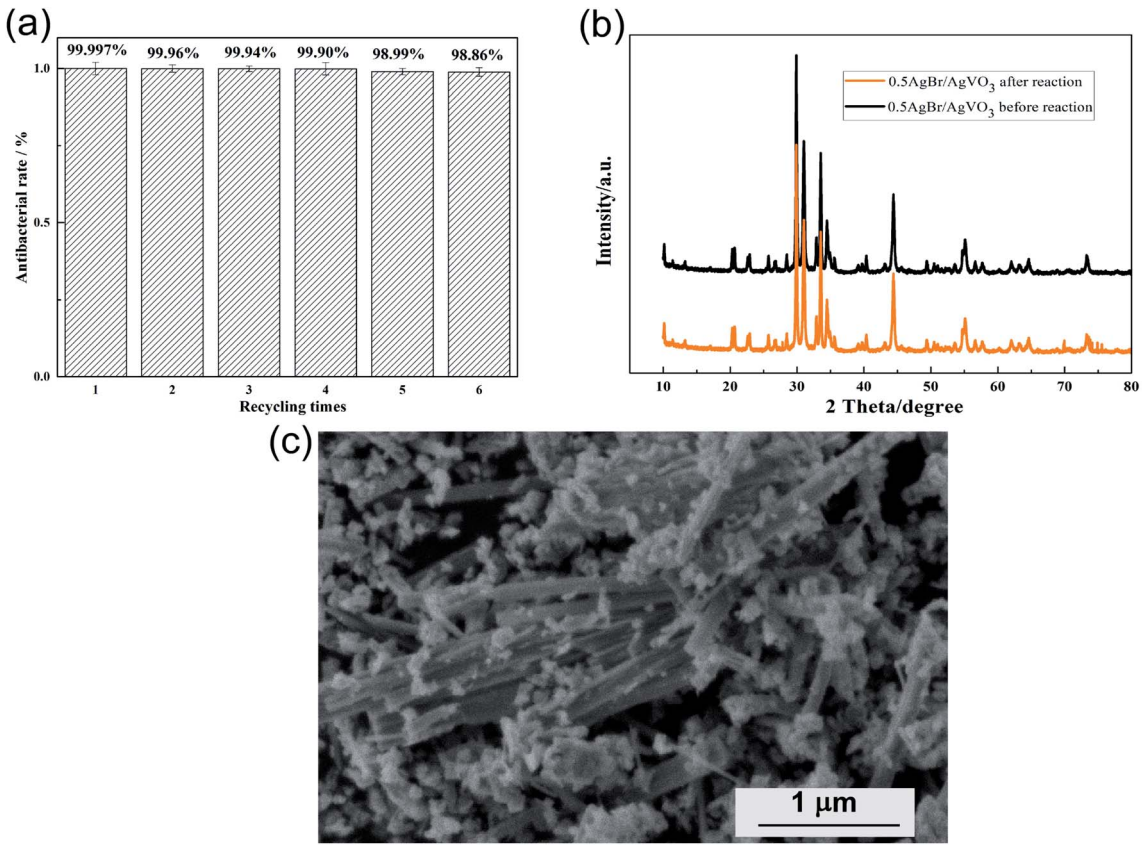

Fig. 8 (a) Recycling photocatalytic antibacterial rates for *P. aeruginosa*; (b) XRD pattern of 0.5AgBr/$AgVO_3$ after six recycling experiments; (c) SEM image of 0.5AgBr/$AgVO_3$ after six recycling experiments under visible light irradiation.

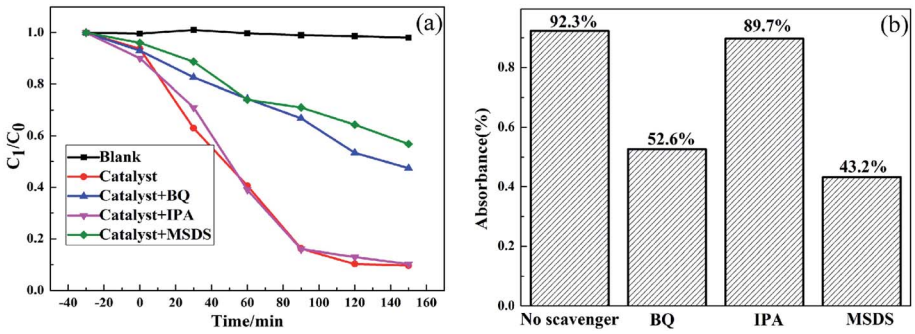

Fig. 9 The active species trapping experiments for degradation of RhB with AgBr/$AgVO_3$ photocatalyst under visible light irradiation.

decreased slightly, suggesting that the $\cdot OH^-$ was not the primary radical species. However, when BQ and MSDS were added, the degradation rates of RhB were 52.6% and 43.2%, respectively, indicating the photocatalytic activity of AgBr/$AgVO_3$ was significantly prohibited. These results suggested that the photocatalytic activity of AgBr/$AgVO_3$ was primarily driven by $\cdot O_2^-$ and h^+.

A possible reaction mechanism was illustrated in Fig. 10. As shown in previous research, silver ions had a bactericidal effect, but the metal silver (Ag^0) which was generated by illumination of $AgVO_3$ would contribute in the separation of electron–hole pairs.[8] And plasmonic enhancements and facile charge transfer resulted from the assistance of metallic Ag, and the SPR effect of Ag nanoparticles played an important role in producing high photocatalytic activity for the oscillation of surface electron.[30,31] At the same time, the conduction band (CB) electrons of noble metals can enhance the reducibility, which decreased the recombination opportunity of e^- and h^+.[32] Additionally, the excellent conductivity of Ag nanoparticles greatly promoted interfacial charge-transfer kinetics among AgBr and $AgVO_3$.

The CB of AgBr (−0.32 eV)[19] was more cathodic than the standard redox potential of $O_2/\cdot O_2^-$ (−0.046 eV *vs.* NHE),[1,12] which exhibited a strong reductive ability and the valence band (VB) of $AgVO_3$ (2.31 eV)[8] had a better oxidation capability. AgBr (2.58 eV)[18,19,24] and $AgVO_3$ (2.03 eV)[8] were matched in their band gap. The energy of visible light was sufficient to excite the VB electrons of $AgVO_3$ and AgBr such that they 'jumped' into the CB.[1,7] At the same time, the energy bands of the two semiconductors would be correspondingly bent and moved. Because of the excellent conductivity of Ag nanoparticles, light-induced

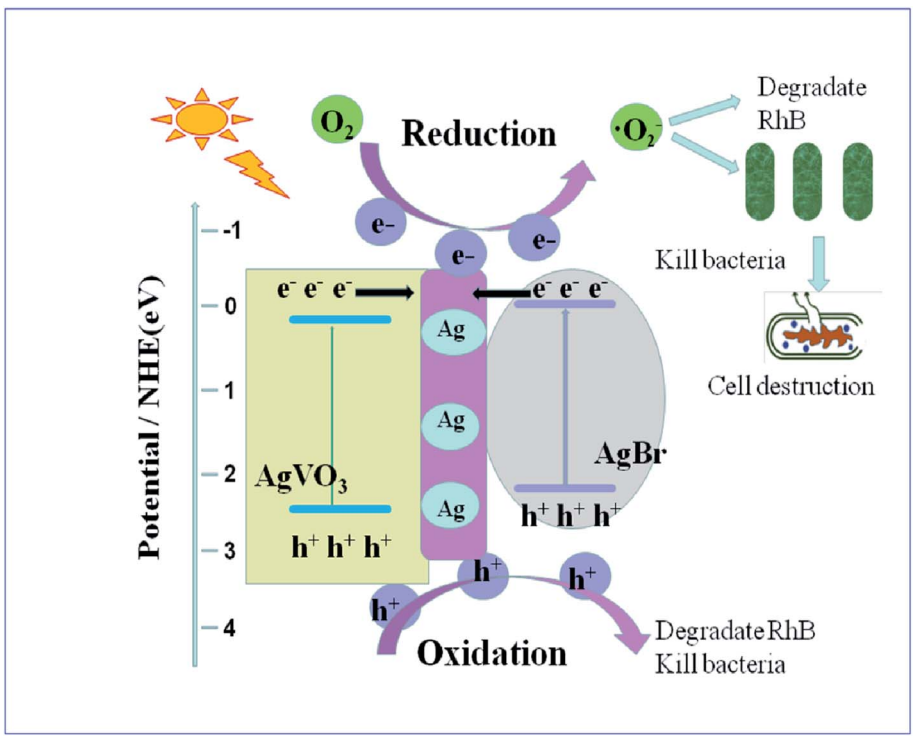

Fig. 10 Schematic diagram of the proposed mechanism.

electrons can be quickly transferred at the interface of the heterostructures, which avoided the recombination with the excited holes. At the same time, these electrons can be captured by oxygen to produce $\cdot O_2^-$ which can attack the cell wall of bacterial,[1] and kill the cell completely,[7,8] revealing the efficient and environmentally friendly advantages of photocatalysis technology. Additionally, the remained holes can be directly oxidized by water to hydroxyl radicals, which played an important role in photocatalytic antibacterial area and water purification applications.

Conclusions

AgBr/$AgVO_3$ photocatalysts were prepared *via* a hydrothermal process and *in situ* growth method, which were composed of rod-shaped $AgVO_3$ and irregular granular AgBr. The photocatalytic experiments indicated that the 0.5AgBr/$AgVO_3$ heterojunction photocatalyst exhibited enhanced photocatalytic activity and antibacterial efficiency, compared to pure AgBr, pure $AgVO_3$ and other AgBr/$AgVO_3$ composites under visible light irradiation. The degradation rate of RhB solution was 92.3% and more than 99.9970% of *E. coli*, *S. aureus* and *P. aeruginosa* cells were killed after 30 min by the photocatalysis of 0.5AgBr/$AgVO_3$. Overall, the 0.5AgBr/$AgVO_3$ heterojunction photocatalyst had excellent photocatalytic activity, stability, reusability and photocatalytic antibacterial performance, which suggested that it could be widely used in photocatalytic antibacterial area and water purification applications.

Authors' contributions

JZ performed the data analysis and modified the manuscript, JW completed the test analysis of XPS and the specific surface area, HHX performed the synthesis and characterization of AgBr/$AgVO_3$ films, JZD and BRH participated in the determination of synthetic schemes, YXZ and XZL participated in the characterization. And HHX supervised the conceptual framework and drafted the manuscript, JZ participated in modifying the manuscript. All authors read and approved the final manuscript.

Availability of data and material

All datasets are presented in the main paper.

Conflicts of interest

The authors declare that they have no competing interests.

Abbreviations

SEM	Scanning electron microscopy
TEM	Transmission electron microscopy
HRTEM	High resolution transmission electron microscopy
XRD	X-ray diffraction
BET	Brunauer–Emmett–Teller
XPS	X-ray photoelectron spectroscopy
UV-DRS	UV-visible diffuse reflectance spectra
RhB	Rhodamine B
IPA	iso-Propyl alcohol
BQ	Benzoquinone
MSDS	Sodium oxalate
VB	Valence band
CB	Conduction band

Acknowledgements

This work is supported by the National Natural Science Foundation of China (Grant No. 41376003 and 41006054), the Strategic Priority Research Program of the Chinese Academy of Sciences, Grant No. XDA13040405, and the National Basic Research Program of China (2014CB643304).

References

1 Y. H. Xiang, P. Ju, Y. Wang, Y. Sun, D. Zhang and J. Q. Yu, *Chem. Eng. J.*, 2016, **288**, 264–275.
2 B. K. Liu, X. L. Han, L. L. Mu, J. T. Zhang and H. Z. Shi, *Mater. Lett.*, 2019, **253**, 148–151.
3 N. Liu, Q. Zhu, N. Zhang, C. Zhang, N. Kawazoe, G. P. Chen, N. Negishi and Y. N. Yang, *Environ. Pollut.*, 2019, **247**, 847–856.
4 L. Gao, Z. H. Li and J. W. Liu, *RSC Adv.*, 2017, **7**, 27515–27521.
5 J. Podporska-Carroll, E. Panaitescu, B. Quilty, L. L. Wang, L. Menon and S. C. Pillaid, *Appl. Catal., B*, 2015, **176–177**, 306–314.
6 X. L. Qin, Y. Huang, K. Wang, T. T. Xu, S. P. Li, M. Zhao, Y. L. Wang and Q. Chen, *Carbon*, 2019, **152**, 459–473.
7 R. A. Senthil, M. Sun, J. Q. Pan, S. Osman, A. Khan and Y. Z. Sun, *Opt. Mater.*, 2019, **92**, 284–293.
8 X. Zhang, J. Zhang, J. Q. Yu, Y. Zhang, Z. X. Cui, Y. Sun and B. R. Hou, *Appl. Catal., B*, 2018, **220**, 57–66.
9 W. Zhao, Y. Guo, Y. Faiz, W. T. Yuan, C. Sun, S. M. Wang, Y. H. Deng, Y. Zhuang, Y. Li, X. M. Wang, H. He and S. G. Yang, *Appl. Catal., B*, 2015, **163**, 288–297.
10 W. Zhao, J. H. Li, Z. B. Wei, S. M. Wang, H. He, C. Sun and S. G. Yang, *Appl. Catal., B*, 2015, **179**, 9–20.
11 Y. Y. Qin, H. Li, J. Lu, Y. S. Yan, Z. Y. Lu and X. L. Liu, *Chin. J. Catal.*, 2018, **39**, 1470–1483.
12 L. Yin, Z. Fu, Y. Li, B. Liu, Z. Lin, J. Lu, X. Chen, X. Han, Y. Deng, W. Hu, D. Zou and C. Zhong, *RSC Adv.*, 2019, **9**, 4521–4529.
13 L. Cao, *Mater. Lett.*, 2017, **188**, 252–256.
14 J. F. Chen, L. Dou, J. Z. Li, B. Chen, J. B. Zhong, J. J. He and R. Duan, *Solid State Sci.*, 2019, **94**, 106–113.
15 X. Zhang, J. Zhang, J. Q. Yu, Y. Zhang, F. K. Yu, L. Jia, Y. L. Tan, Y. M. Zhu and B. R. Hou, *J. Colloid Interface Sci.*, 2019, **533**, 358–368.
16 P. Mahsa and H. Aziz, *J. Colloid Interface Sci.*, 2017, **491**, 216–229.
17 Y. Bai, Q. Xu and Z. S. Cai, *J. Mater. Sci.: Mater. Electron.*, 2018, **29**, 17580–17590.

18 Y. J. Liu, F. Zhou, S. Zhan and Y. F. Yang, *J. Inorg. Organomet. Polym.*, 2017, **27**, 1365–1375.
19 F. Guo, W. L. Shi, Y. Cai, S. W. Shao, T. Zhang, W. S. Guan, H. Huang and Y. Liu, *RSC Adv.*, 2016, **6**, 93887–93893.
20 L. L. Lai, W. Wen, B. Fu, X. Y. Qian, J. B. Liu and J. M. Wu, *Mater. Des.*, 2016, **108**, 581–589.
21 S. Talebzadeh, F. Forato, B. Bujoli, S. A. Trammell, S. Grolleau, H. Pal, C. Queffélec and D. A. Knight, *RSC Adv.*, 2018, **8**, 42346–42352.
22 Q. E. Zhao, W. Wen, Y. Xia and J. M. Wu, *J. Phys. Chem. Solids*, 2019, **124**, 192–198.
23 Y. Xu, W. Wen and J. M. Wu, *J. Hazard. Mater.*, 2018, **343**, 285–297.
24 X. Miao, Z. Y. Ji, J. J. Wu, X. Shen, J. Wang, L. Kong, M. Liu and C. Song, *J. Colloid Interface Sci.*, 2017, **502**, 24–32.
25 Q. Jin, W. Wen, J. Q. Bai and J. M. Wu, *Thin Solid Films*, 2019, **683**, 111–117.
26 Y. D. Meng, Y. Z. Hong, C. Y. Huang and W. D. Shi, *CrystEngComm*, 2017, **19**, 982–993.
27 S. Xue, Z. W. Wei, X. Y. Hou, W. H. Xie, S. Y. Li, X. N. Shang and D. Y. He, *Appl. Surf. Sci.*, 2015, **355**, 1107–1115.
28 S. Mosleh, K. Dashtian, M. Ghaedi and M. Amiri, *RSC Adv.*, 2019, **9**, 30100–30111.
29 T. Jan, S. Azmat, B. Wahid, M. Adil, H. Alawadhi, Q. Mansoor, Z. Farooq, S. Z. Ilyas, I. Ahmad and M. Ismail, *Mater. Sci. Semicond. Process.*, 2018, **84**, 71–74.
30 H. B. Zeng, W. P. Cai, P. S. Liu, X. X. Xu, H. J. Zhou, C. Klingshirn and H. Kalt, *ACS Nano*, 2008, **2**, 1661–1670.
31 C. Hu, Y. Q. Lan, J. H. Qu, X. X. Hu and A. M. Wang, *J. Phys. Chem. B*, 2006, **110**, 4066–4072.
32 L. J. Wang, X. W. Yan, C. L. Xu, Z. L. Xiao, L. M. Yang, B. Zhang and Q. Q. Wang, *Analyst*, 2011, **136**, 1221–1229.